analytical chemistry

pubs.acs.org/ac Article

Detection of Matrix Metalloproteinase 2 by a Polypeptide Cleavable Split-Type Sensor Based on Atomically Precise Bimetallic Nanocluster $Au_3Ag_5(MSA)_3$

Qi Zhu, Xu Sun, Yu Du,* Xiaoyue Zhang,* Xiang Ren, Hongmin Ma, Dan Wu, Huangxian Ju, and Qin Wei*

Cite This: *Anal. Chem.* 2025, 97, 14574−14583 Read Online

ACCESS | Metrics & More | Article Recommendations | Supporting Information

ABSTRACT: In this study, a split-type electrochemiluminescence (ECL) sensor based on polypeptide cleavage was proposed for the sensitive detection of matrix metalloproteinase 2 (MMP 2). The bimetallic nanoclusters were protected by mercaptosuccinic acid (MSA), named $Au_3Ag_5(MSA)_3$, serving as a signal probe. Owing to the synergistic effect of the bimetal composition, the clusters exhibited enhanced ECL properties. Polypeptide chains (PLGVR) that can be specifically cleaved by MMP 2 were selected from the MMP 2 domain. Additionally, the antifouling segment (PPEKEK) and the binding segment (CCC) were incorporated into the polypeptide chain design. In the presence of MMP 2, a specific cleavage site on the polypeptide was targeted, resulting in the detachment of $Au_3Ag_5(MSA)_3$ and subsequent generation of an ECL signal. Compared to conventional detection methods, this approach exhibited enhanced sensitivity and improved stability. This method provides a valuable reference for detecting members of the matrix metalloproteinase family and holds promising prospects for future development.

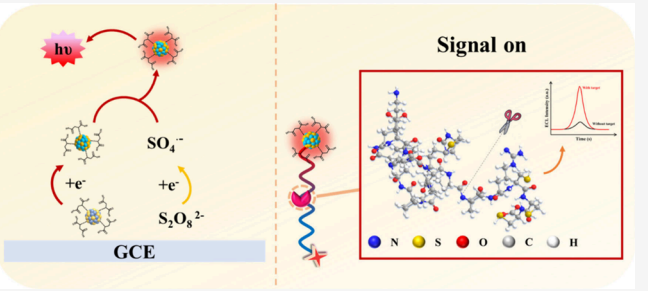

INTRODUCTION

Matrix metalloproteinases (MMPs) are a family of zinc-dependent endopeptidases. MMPs possess the capacity to break down virtually all protein substrates found in the extracellular matrix (ECM). MMPs can promote the degradation and remodeling of the extracellular matrix and exert a dominant influence in regulating reproduction, facilitating the restructuring of tissues and guiding morphogenesis.[1,2] Matrix metalloproteinase 2 (MMP 2) stands as a prominent member of the MMPs family, capable of selectively cleaving a wide range of protein substrates.[3,4] MMP 2 effectively dismantles the histological barriers that tumor cells encounter during invasion, thereby exerting a pivotal influence on tumor progression and metastasis.[5,6] Therefore, the detection of MMP 2 is of considerable importance for diagnosing and treating various diseases. At present, a variety of detection methods and technologies for MMP 2 have been developed. In addition to traditional immunohistochemistry (IHC),[7] various methods such as enzyme-linked immunosorbent assays (ELISA)[8] and zymography[9] have already been developed. Furthermore, a diverse array of sensors based on electrochemiluminescence (ECL),[10] photoelectrochemical (PEC),[11] fluorescence (FL),[12] and surface-enhanced Raman spectroscopy (SERS)[13] have also undergone continuously progress. The ECL sensor has been better used in the detection of MMP 2 due to its advantages of simple preparation, cost-effectiveness and high sensitivity.[14]

ECL is a phenomenon that causes chemiluminescence by electrochemical methods.[15] The ECL sensor employs electrodes as conversion elements, utilizing immobilized carriers to anchor antigens, antibodies, enzymes, hormones, and other biosensitive substances. Additionally, the organism itself can serve as a sensitive element on the electrode.[16] Through the specific recognition between biomolecules, the reaction signal of the target molecule is converted into an electrical signal and recorded for the detection of the target analyte.[17,18] Because of its outstanding sensitivity, low background, superior selectivity, and strong controllability, the ECL sensor has found extensive application in disease diagnosis and various other domains.[19,20] Among them, ECL luminophores serve as a pivotal component for generating optical signals. ECL luminophores directly influence application strategies and efficiency, and plays a vital role in the construction of sensors.[21]

Received: April 3, 2025
Revised: June 27, 2025
Accepted: June 27, 2025
Published: July 4, 2025

https://doi.org/10.1021/acs.analchem.5c02007
Anal. Chem. 2025, 97, 14574−14583

Scheme 1. Schematic Diagram of the Preparation Process of the Biotin−PPEKEKPLGVRCCC-$Au_3Ag_5(MSA)_3$ (A) and the ECL Sensing Platform (B)

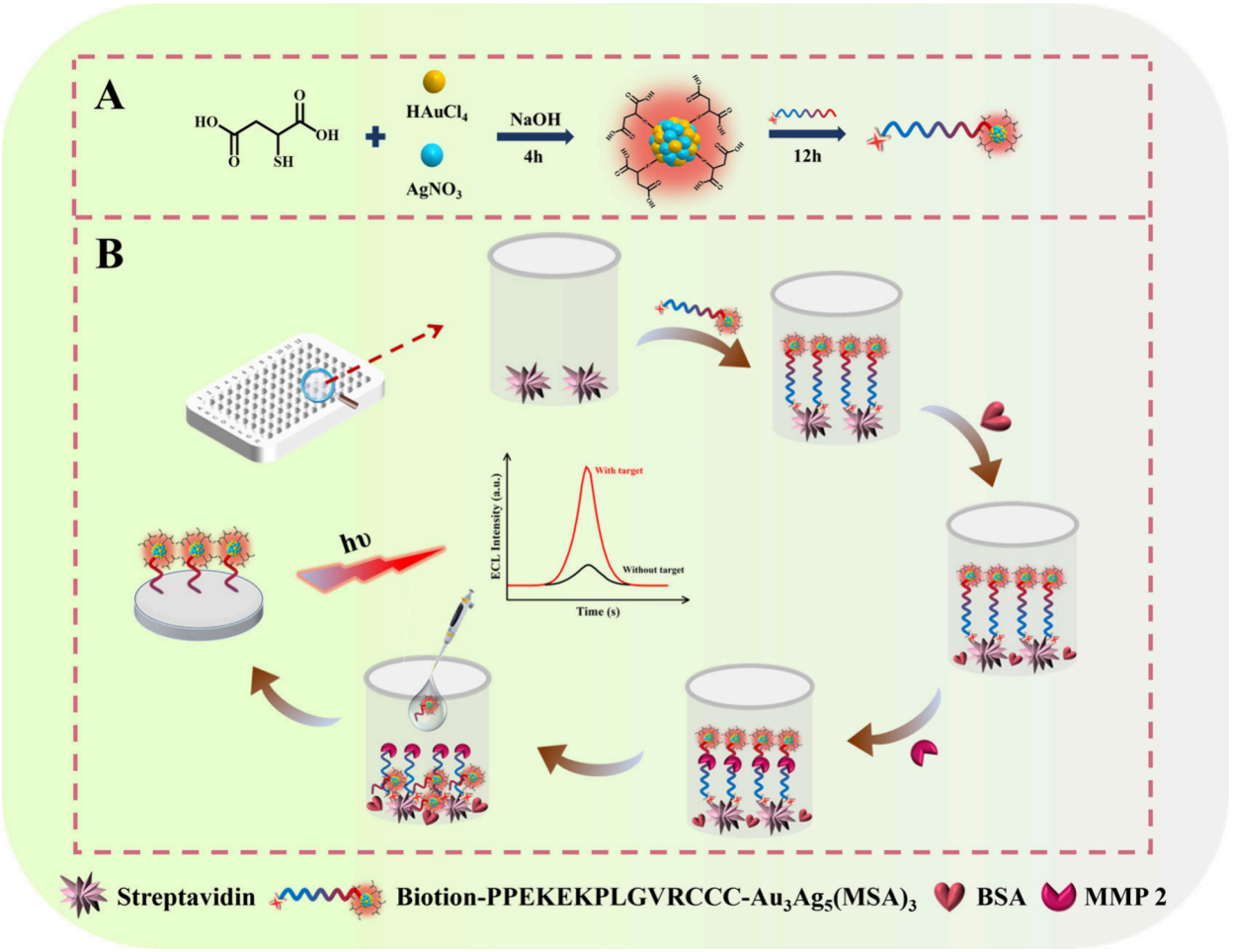

Metal nanoclusters (NCs) have a size comparable to the Fermi wavelength.[22] As nanoscale materials, their unique size effects give metallic NCs molecular properties, such as splitting states of continuous density into discrete energy levels.[23,24] Compared to single NCs, bimetallic NCs exhibit synergistic effects that typically result in enhanced luminous efficiency and increased luminous intensity.[25,26] This improvement arises from the synergistic effect between different metals, which optimizes the electron transfer process and enhances the quantum yield of luminescence.[27] Au NCs have garnered significant concern owing to distinctive chemical and optical characteristics, low biotoxicity, and exceptional biological compatibility.[28] Nevertheless, the restricted ECL efficiency of Au NCs poses limitations on their practical application. Recent studies indicated that bimetallic nanoclusters combining gold and silver atoms can enhance the ECL signal and stability.[29,30] This enhancement arises from the interaction between the electrons of the two metals, changing the electronic structure of the nanoclusters to form electron and geometrically stable nanoclusters.[31] Meanwhile, by incorporating atoms with distinct properties, the intramolecular vibrations and rotations of the ligands were effectively suppressed, thereby hindering nonradiative relaxation of the excited states.[29]

In this study, the atomically precise bimetallic nanocluster protected by mercaptosuccinic acid (MSA), named $Au_3Ag_5(MSA)_3$, was synthesized by adding silver atoms to gold atoms. By increasing radiative relaxation of excited states, the emission intensity, stability, and ECL efficiency of $Au_3Ag_5(MSA)_3$ were significantly improved. To achieve efficient detection of MMP 2, we constructed a split-type ECL sensor based on peptide cleavage utilizing an enzyme digestion method. The $Au_3Ag_5(MSA)_3$ served as the signal probe. Meanwhile, a polypeptide (Biotion−PPEKEKPLGVR-CCC) was designed, and the Biotion was added to the link section of the polypeptide for connecting with the 96-well microplates coated with streptavidin. An antifouling section (PPEKEK) was designed to eliminate charge attraction and exclude hydrophobic effects.[32] The thiol group contained in the terminal cysteine (CCC) was used to connect the luminous $Au_3Ag_5(MSA)_3$ by Au−S and Ag−S bonds. Due to the introduction of MMP 2, the specific site within the polypeptide was cleaved, resulting in the generation of ECL signals as $Au_3Ag_5(MSA)_3$ was released. This provided a new idea for the detection of MMP 2 in clinical research and biomedicine.

EXPERIMENTAL SECTION

Preparation of $Au_3Ag_5(MSA)_3$. The preparation of $Au_3Ag_5(MSA)_3$ was slightly modified on the basis of the previously reported literature.[33] Initially, in 10 mL of ultrapure water, 9.4 mg of MSA and 200 μL of NaOH (1 M) were introduced with strong agitation. Subsequently, 68 μL of

https://doi.org/10.1021/acs.analchem.5c02007
Anal. Chem. 2025, 97, 14574−14583

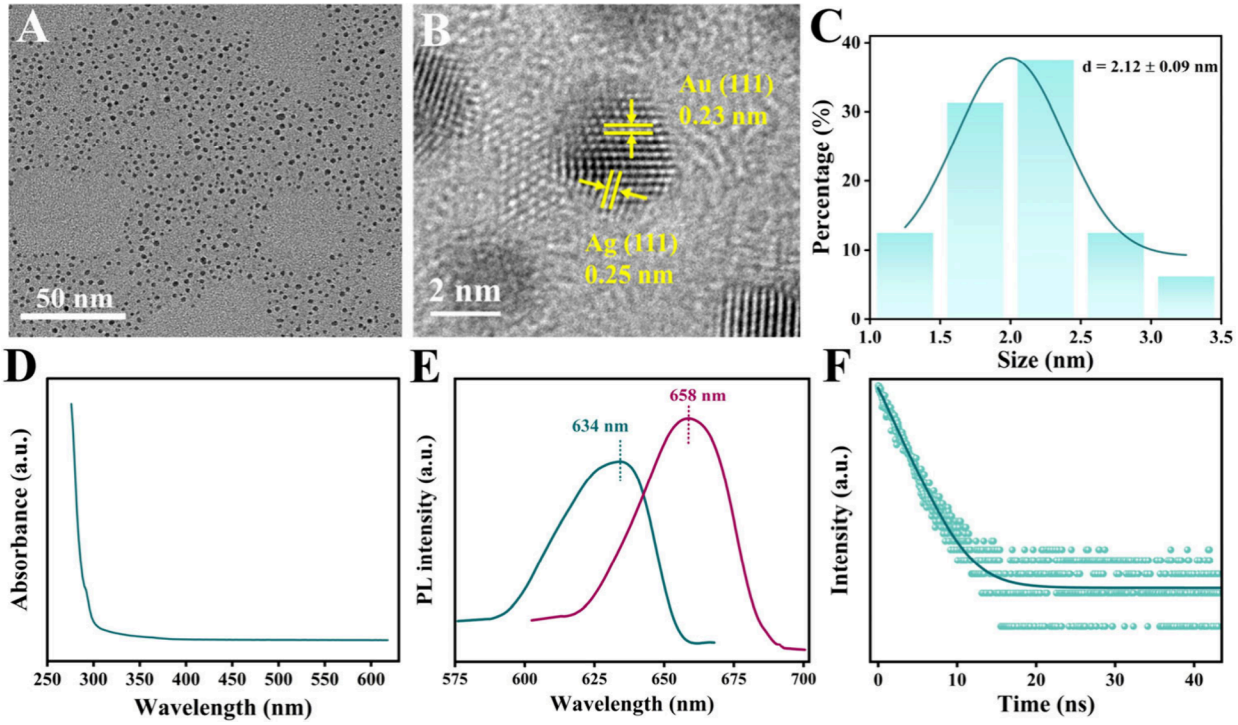

Figure 1. TEM image (A), HRTEM image (B), size distribution (C), and UV−vis absorption diagram (D) of $Au_3Ag_5(MSA)_3$. PL emission spectrum of MSA-Au NCs (green curve) and $Au_3Ag_5(MSA)_3$ (red curve) (E). Fluorescence lifetime of $Au_3Ag_5(MSA)_3$ (F).

$AgNO_3$ (0.1 M), 2.8 mL of $HAuCl_4$ (24.3 mM) and 300 μL of NaOH (1 M) were added to the solution for 15 min under stirring at 500 rpm. Then, 140 μL of $NaBH_4$ (0.5 mg/mL) was added in a single dose. Then continued to stir for 4 h to get a brown black solution. All of the experimental procedures were conducted at room temperature.

Construction of ECL Sensor. Initially, 500 μL of Biotin−PPEKEKPLGVRCCC (0.56 mM) was added to 500 μL of $Au_3Ag_5(MSA)_3$ (5.0 mM) and incubated overnight with oscillations at room temperature. Then, 50 μL of the mixture was added to the 96-well microplate coated with streptavidin, which was then positioned on a horizontal shaker and incubated at 25 °C for 1.5 h. Then the solution was sucked out, and 100 μL of phosphate buffered saline (PBS) was added to the plate. The microplate was placed on a horizontal shaker and shaken for 5 min, the liquid was sucked out of the microwells, and this washing step was repeated 3 times. Then, 50 μL of PBS with a 5% concentration of bovine serum albumin (BSA) was added to the microwells to block other nonspecific active sites. The plate was positioned on the horizontal shaking device and incubated for 1 h. Then the solution in the plate was sucked out, and 100 μL of PBS was added with shaking on a horizontal shaker for 5 min. The supernatant was sucked out in the microwells, and washing was repeated 3 times. Subsequently, 50 μL of MMP 2 with diverse concentrations were dispensed into microplate with incubating for 3 h. The liquid from the microplate was then sucked out and mixed in a centrifuge tube with a solution washed with 100 μL of PBS. Subsequently, 10 μL of solution from the centrifuge tube was drawn and dripped onto the polished glass carbon electrode (GCE). Scheme 1 describes the specific construction process of the sensor.

RESULTS AND DISCUSSION

Characterization of $Au_3Ag_5(MSA)_3$. The morphology of $Au_3Ag_5(MSA)_3$ was characterized by transmission electron microscope (TEM). The particle diameter of $Au_3Ag_5(MSA)_3$ was approximately 2.12 nm, with small size, uniform distribution and excellent dispersion (Figure 1A,C). The lattice structure of the $Au_3Ag_5(MSA)_3$ was characterized by a high resolution transmission electron microscope (HRTEM). As depicted in Figure 1B, the lattice fringe of 0.23 nm corresponded to the (111) crystal plane of Au, while the 0.25 nm lattice fringe was associated with the (111) crystal plane of Ag. This observation confirmed that silver atoms and gold atoms had successfully combined. As depicted in the UV−vis absorption diagram of $Au_3Ag_5(MSA)_3$ (Figure 1D), the ultraviolet absorption of $Au_3Ag_5(MSA)_3$ decreased significantly with the increase of wavelength. Meanwhile, there was no characteristic absorption peak of the Au nanoparticle when the wavelength was around 520 nm. Moreover, there was no UV absorption peak of the Ag nanoparticle at 420 nm, which indicated that the synthesized $Au_3Ag_5(MSA)_3$ had a smaller size. As depicted in Figure 1E, the fluorescence spectrum indicated that the emission peak of the MSA-Au NCs was located at 634 nm. When silver atoms were added, the emission wavelength of the $Au_3Ag_5(MSA)_3$ was red-shifted by 24 nm, and the optimal emission wavelength was about 658 nm. The optimal excitation wavelength (Figure S1) appeared at around 486 nm. The fluorescence lifetime decay curves of $Au_3Ag_5(MSA)_3$ (Figure 1F) and MSA-Au NCs (Figure S2) conformed to the double exponential model. The fluorescence lifetime of MSA-Au NCs was 1.33 ns, while that of $Au_3Ag_5(MSA)_3$ was 2.71 ns. This observation may be explained by the capacity of Ag atoms to inhibit the nonradiative relaxation processes of the excited state, thereby extending the fluorescence lifetime of the nanoclusters.

https://doi.org/10.1021/acs.analchem.5c02007
Anal. Chem. 2025, 97, 14574−14583

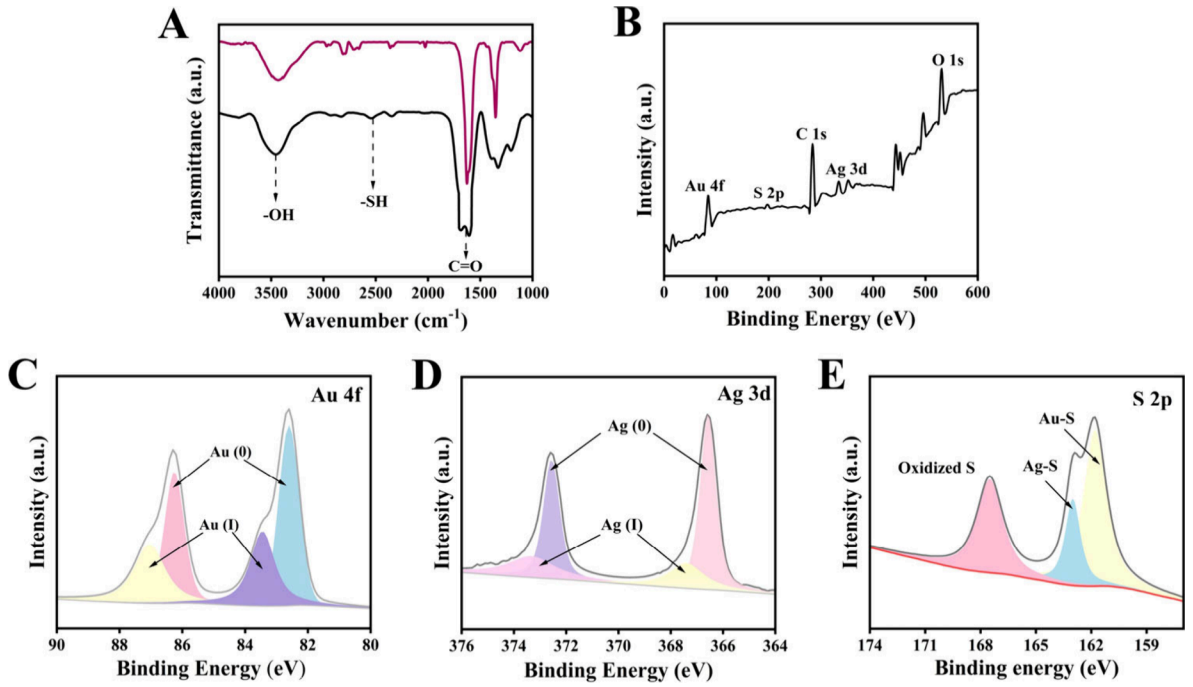

Figure 2. Infrared spectra of MSA (black curve) and $Au_3Ag_5(MSA)_3$ (red curve) (A). XPS spectra of the whole region (B), the Au 4f region (C), the Ag 3d region (D), and the S 2p region (E) of $Au_3Ag_5(MSA)_3$.

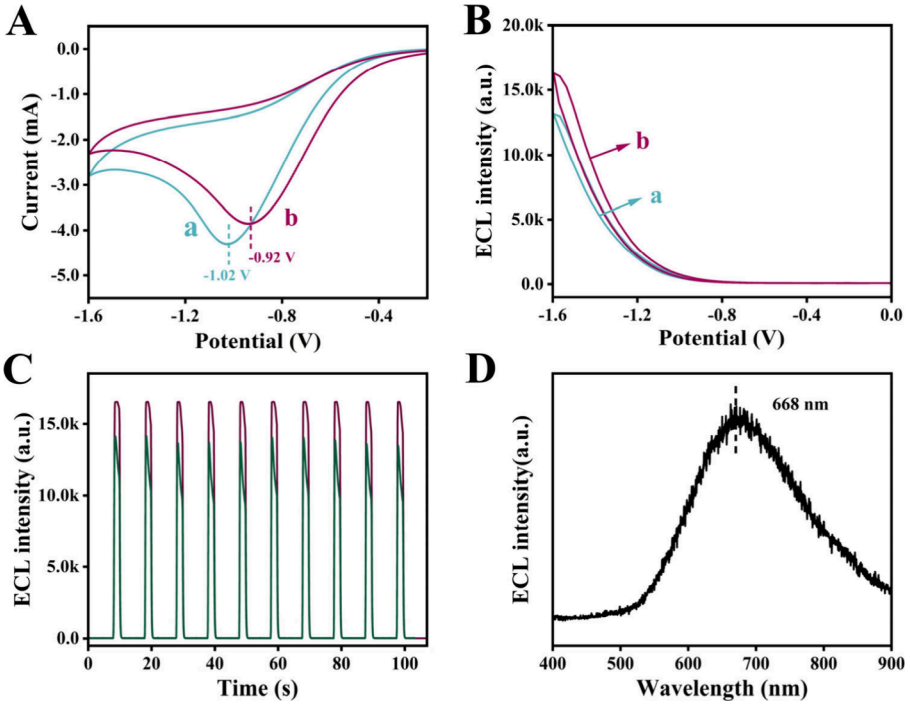

Figure 3. CV curves (A), ECL−potential curves (B) and ECL−time (C) of MSA-Au NCs (green curve) and $Au_3Ag_5(MSA)_3$ (red curve) in PBS containing 100 mM $S_2O_8^{2-}$. ECL emission (D) curve of $Au_3Ag_5(MSA)_3$ in saturated N_2 treated PBS containing 100 mM $S_2O_8^{2-}$.

The infrared spectra of $Au_3Ag_5(MSA)_3$ and MSA were respectively characterized. As shown in Figure 2A, a characteristic sulfhydryl peak at 2550 cm^{-1} was observed in the infrared spectrum of MSA, while no such peak was detected in the spectrum of $Au_3Ag_5(MSA)_3$. This result showed that the sulfhydryl groups in MSA were completely bound to the surface of the nanoclusters by Au−S and Ag−S bonds. X-ray photoelectron spectroscopy (XPS) was used to characterize $Au_3Ag_5(MSA)_3$. The total XPS spectrum (Figure 2B) showed the correlation peaks of Au (4f), Ag (3d), S (2p), O (1s), and C (1s). As shown in Figure 2C, the Au peaks (4f) were divided into two different peaks. The peak of Au (4f) was divided into two distinct peaks, namely, Au $4f_{7/2}$ (82.6 eV) and Au $4f_{5/2}$ (86.3 eV) of Au(0) and Au $4f_{7/2}$ (83.5 eV) and Au $4f_{5/2}$ (87.1 eV) of Au(I). This showed that Au(I) and Au(0) coexist in $Au_3Ag_5(MSA)_3$, and the presence of Au(I) helped to improve the stability of the nanoclusters. Figure 2D shows that the peaks of Ag (3d) were divided into two distinct peaks, Ag(0)

https://doi.org/10.1021/acs.analchem.5c02007
Anal. Chem. 2025, 97, 14574−14583

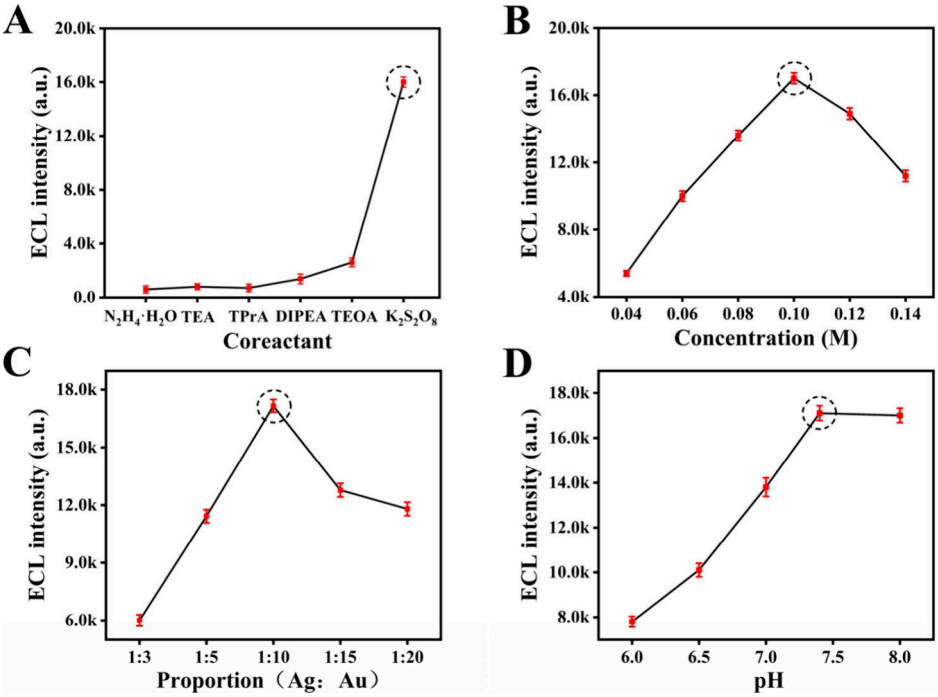

Figure 4. Optimization of types of co-reactants in same concentration (A), concentrations of $K_2S_2O_8$ (B), proportion of Ag atoms and Au atoms (C) and pH of PBS (D). Error bars: ± standard deviation (SD), n = 3.

of Ag $3d_{5/2}$ (366.6 eV) and Ag $3d_{3/2}$ (372.6 eV) and Ag(I) of Ag $4f_{5/2}$ (367.4 eV) and Ag $3d_{3/2}$ (373.4 eV), respectively. As shown in Figure 2E, the characteristic peaks of S 2p confirmed Au−S and Ag−S covalent bonds. O 1s (Figure S3A) showed that the carboxyl group in the ligand MSA formed a coordination bond of COO−Ag with Ag atoms, indicating that the presence of silver atoms inhibited the nonradiative motion of the nanoclusters.[34]

Electrochemical and ECL Properties of $Au_3Ag_5(MSA)_3$. ECL tests were performed in PBS solution with pH 7.4 and a $K_2S_2O_8$ concentration of 0.1 M. The cyclic voltammetry (CV) (Figure 3A) illustrated that when only Au NCs existed, MSA-Au NCs had a reduction peak at −1.02 V. When Ag atoms were introduced to the central atoms, the reduction peak of $Au_3Ag_5(MSA)_3$ was −0.92 V, and the reduction peak moved in the positive direction. As shown in Figure 3B,C, the ECL signal of $Au_3Ag_5(MSA)_3$ was enhanced by approximately 1.3 times relative to that of MSA-Au NCs. Concurrently, the ECL signal of $Au_3Ag_5(MSA)_3$ demonstrated a greater stability. It was confirmed that the presence of Ag atoms reduced the reduction potential of $Au_3Ag_5(MSA)_3$ and enhanced the ECL signal strength and stability. This phenomenon could be attributed to the improved charge transfer of the bimetallic and the suppression of nonradiative relaxation processes in the nanoclusters.[35] The ECL emission of $Au_3Ag_5(MSA)_3$ was distinctly observed, peaking at a wavelength of 668 nm (Figure 3D). Compared with the fluorescence wavelength, the ECL wavelength showed a red shift of 10 nm. This demonstrated that the ECL emission of $Au_3Ag_5(MSA)_3$ was surface state emission.

Optimization of ECL Test Conditions for $Au_3Ag_5(MSA)_3$. To investigate the influence of different conditions on the ECL signal of $Au_3Ag_5(MSA)_3$, several key factors were optimized. Figure 4A shows the effects of different co-reactants on ECL signals. In the context of anodic co-reactants, like triethylamine (TEA), tri-*n*-propylamine (TPrA) and triethanolamine (TEOA), $Au_3Ag_5(MSA)_3$ emitted smaller ECL signals. When $K_2S_2O_8$ was used as the co-reactant, $Au_3Ag_5(MSA)_3$ exhibited a stronger ECL signal than other co-reactants at the same concentration. Consequently, $Au_3Ag_5(MSA)_3$ was deemed to be a cathode luminescent material in this context. As shown in Figure 4B, the ECL intensity reached its maximum when the concentration of $K_2S_2O_8$ was increased to 0.1 M. However, further increasing the concentration beyond 0.1 M resulted in a decrease in the ECL signal. Therefore, 0.1 M $K_2S_2O_8$ was the optimal concentration for ECL testing. As shown in Figure 4C, the ECL signal was at its maximum when the ratio of Ag to Au atoms was 1:10. The ECL signals gradually increased as the pH increased in the range 6.0−7.4 (Figure 4D), reaching a maximum ECL signal when the pH value was 7.4. At pH 8.0, the ECL signal remained relatively unchanged compared to its level at a pH of 7.4. However, a pH of 7.4 provided a suitable environment for subsequent enzymatic digestion reactions. Therefore, 7.4 was selected as the optimal pH value.

ECL Efficiency of $Au_3Ag_5(MSA)_3$. Using $Ru(bpy)_3^{2+}$ solution as a reference, the ECL efficiency of $Au_3Ag_5(MSA)_3$ was calculated. ECL efficiency was calculated by the following formula:

$$\varphi_{ECL} = \varphi^{\Theta}_{ECL}(I/Q)/(I^{\Theta}/Q^{\Theta})$$

φ^{Θ}_{ECL} is the ECL efficiency of $Ru(bpy)_3^{2+}$, set to 5%. I^{Θ} and Q^{Θ} represent the ECL signal value of $Ru(bpy)_3^{2+}$ and the consumed charge (integration of current and time). Respectively, I and Q represent the ECL signal value and the consumed charge of $Au_3Ag_5(MSA)_3$. The ECL efficiency of $Au_3Ag_5(MSA)_3$ was 3.55%, while the ECL efficiency of MSA-Au NCs was 2.98%. Therefore, the incorporation of silver atoms effectively enhanced the ECL efficiency.

Possible Cathodic ECL Mechanism. To illustrate the luminescence mechanism of the $Au_3Ag_5(MSA)_3/K_2S_2O_8$

https://doi.org/10.1021/acs.analchem.5c02007
Anal. Chem. 2025, 97, 14574−14583

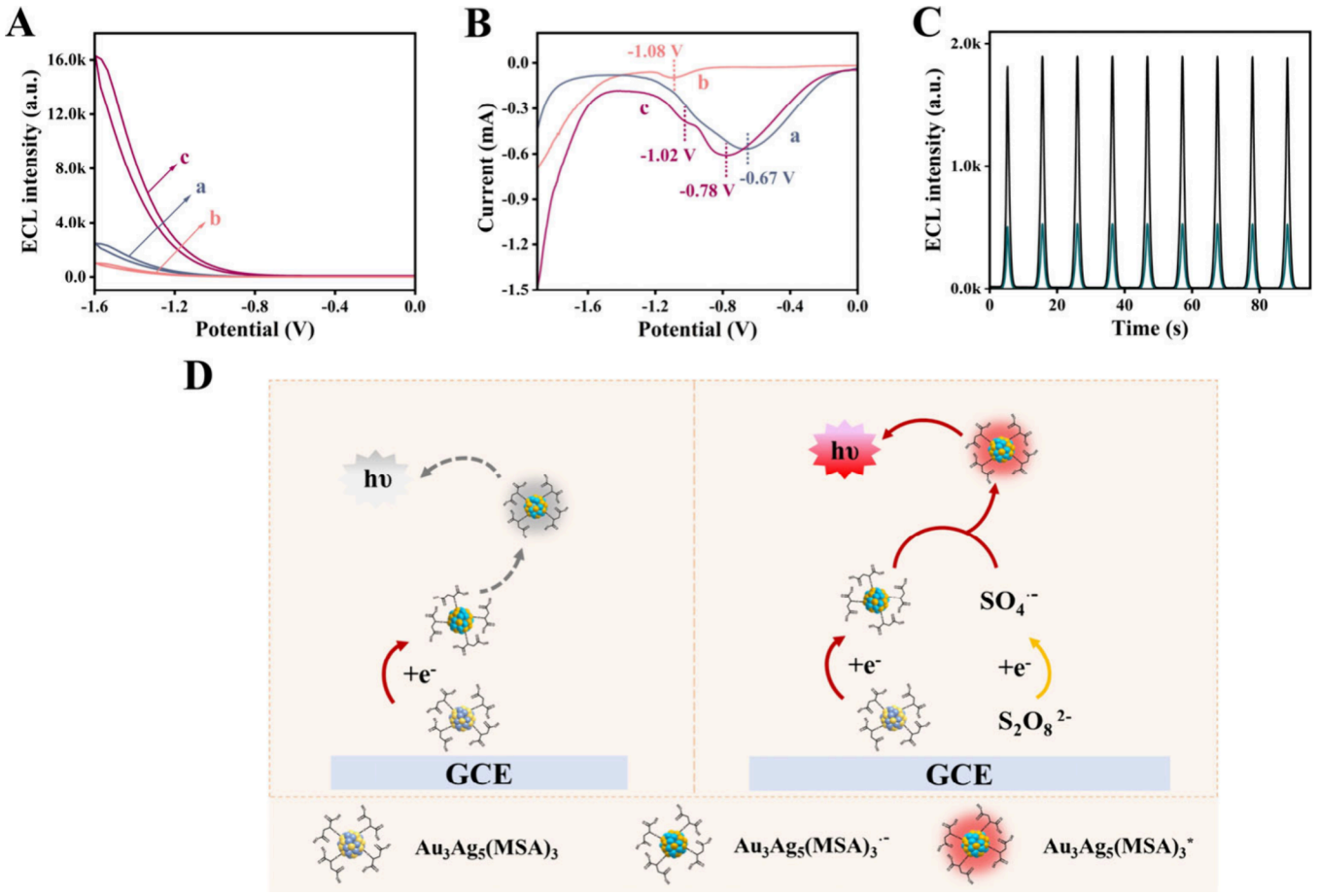

Figure 5. ECL−potential (A) and DPV curves (B) of (a) GCE in PBS containing 100 mM $S_2O_8^{2-}$, (b) $Au_3Ag_5(MSA)_3$ in pure PBS, and (c) $Au_3Ag_5(MSA)_3$ in PBS containing 100 mM $S_2O_8^{2-}$. ECL−time curves of GCE in PBS containing 100 mM $S_2O_8^{2-}$ (black curve) and saturated N_2 treated PBS containing 100 mM $S_2O_8^{2-}$ (green curve) (C). Schematic diagram of the ECL mechanism (D).

system, a thorough investigation of their ECL−potential and DPV (differential pulse voltammetry) was conducted. Figure 5A shows that the bare electrode generated a relatively low ECL signal in $K_2S_2O_8$ (curve a). This signal was attributed to the interaction between $K_2S_2O_8$ and dissolved oxygen. This viewpoint was supported by Figure 5C, where the ECL signal in N_2-saturated $K_2S_2O_8$ was approximately 500 au. However, the ECL signal was enhanced to 1900 au in $K_2S_2O_8$ without N_2 treatment. $Au_3Ag_5(MSA)_3$ had no significant ECL signal in PBS (curve b). However, $Au_3Ag_5(MSA)_3$ generated the strongest ECL signal in $K_2S_2O_8$ solution, reaching 16200 au (curve c).

As shown in Figure 5B, the bare electrode in $K_2S_2O_8$ exhibited a reduction peak at around −0.67 V (curve a). In pure PBS, $Au_3Ag_5(MSA)_3$ showed a reduction peak at approximately −1.08 V (curve b). In the $K_2S_2O_8$ solution, $Au_3Ag_5(MSA)_3$ displayed two reduction peaks (curve c) at −0.78 and −1.02 V, corresponding to the reduction of $K_2S_2O_8$ and $Au_3Ag_5(MSA)_3$, respectively. Therefore, the reaction mechanism was likely as illustrated in Figure 5D. First, $K_2S_2O_8$ gained electrons and was preferentially reduced to form the oxidizing radical $SO_4^{\bullet-}$ (eq 1). Then, $Au_3Ag_5(MSA)_3$ underwent reduction by acquiring electrons, generating $Au_3Ag_5(MSA)_3^{\bullet-}$ (eq 2). Subsequently, $Au_3Ag_5(MSA)_3^{\bullet-}$ interacted with $SO_4^{\bullet-}$ to form the excited state $Au_3Ag_5(MSA)_3$* (eq 3). Finally, $Au_3Ag_5(MSA)_3$* transitioned back to its ground state, emitting ECL emission (eq 4). Possible reaction mechanisms were as follows:

$$S_2O_8^{2-} + e^- \rightarrow SO_4^{\bullet-} + SO_4^{2-} \quad (1)$$

$$Au_3Ag_5(MSA)_3 + e^- \rightarrow Au_3Ag_5(MSA)_3^{\bullet-} \quad (2)$$

$$Au_3Ag_5(MSA)_3^{\bullet-} + SO_4^{\bullet-} \rightarrow Au_3Ag_5(MSA)_3^{*} + SO_4^{2-} \quad (3)$$

$$Au_3Ag_5(MSA)_3^{*} \rightarrow Au_3Ag_5(MSA)_3 + h\nu \quad (4)$$

Antifouling Performance of Biotin−PPEKEKPLGVR-CCC. The pollution of the sensor mainly comes from nonspecific adsorption.[36] It has been revealed that polypeptides with biocompatibility and hydrophilicity can effectively resist the adsorption of nonspecific biomolecules. They were widely used as antifouling materials.[37] The antifouling capability of the polypeptide was assessed by comparing DPV responses of various electrode interfaces following a 30 min incubation in fetal bovine serum (FBS) solution. The DPV signal exhibited a significant reduction of approximately 48% following the incubation of the bare electrode with varying concentrations of FBS solution (Figure 6A,B). The DPV signal of the polypeptide-modified electrode decreased by about 23%. The results demonstrated that the polypeptide-modified electrode exhibited superior antipollution performance compared to the bare electrode. The antifouling performance of

https://doi.org/10.1021/acs.analchem.5c02007
Anal. Chem. 2025, 97, 14574−14583

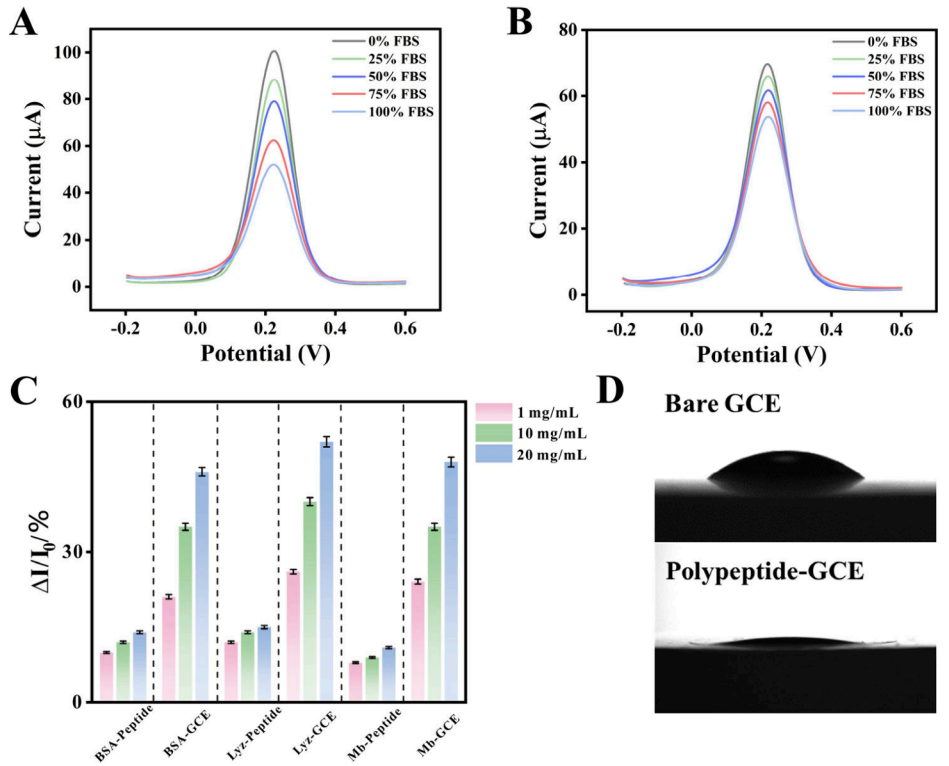

Figure 6. DPV response of bare GCE (A) and GCE with polypeptide (B) in 0.1 M PBS containing 5 mM $[Fe(CN)_6]^{3-/4-}$ after incubation in various concentrations of FBS (0−100%). Response changes of bare GCE and polypeptide with GCE in different protein solutions (C). Water contact angles on bare GCE and GCE with the polypeptide (D). Error bars: ± standard deviation (SD), n = 3.

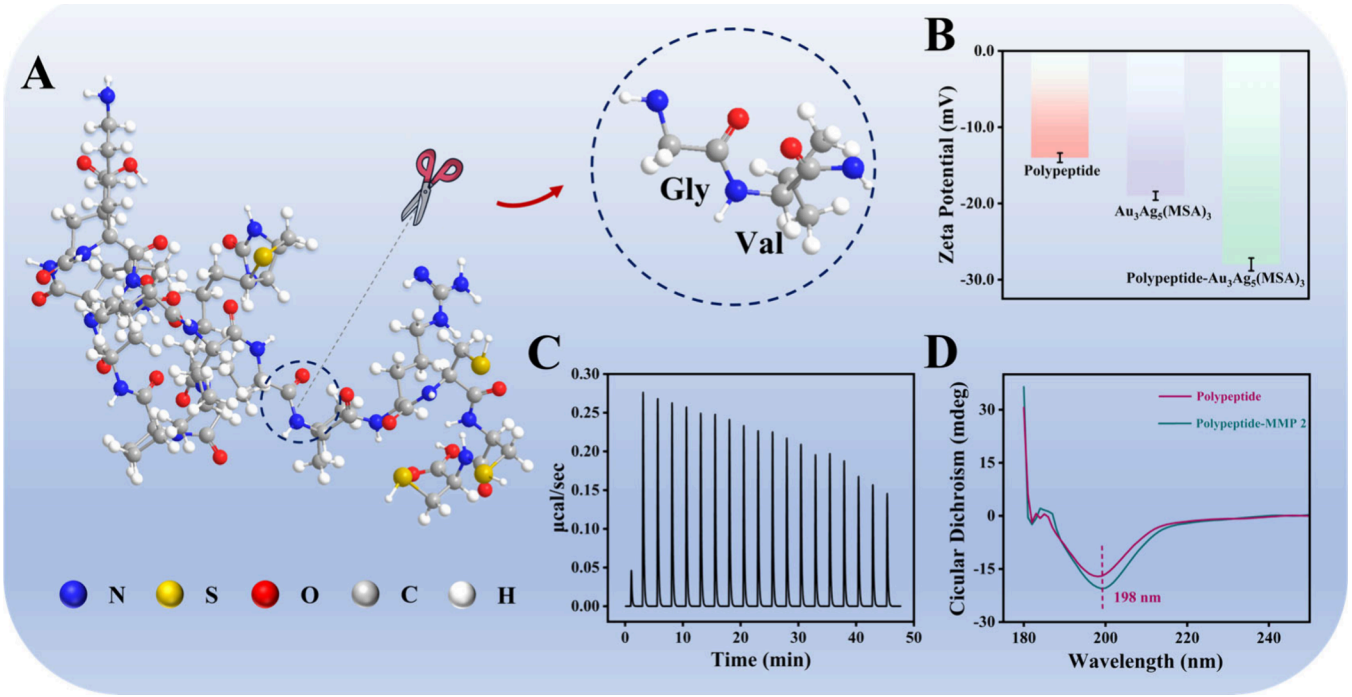

Figure 7. Cleavage site of MMP 2 for the designed polypeptide chain (A). The zeta-potential values of PPEKEKPLGVRCCC, $Au_3Ag_5(MSA)_3$, and PPEKEKPLGVRCCC-$Au_3Ag_5(MSA)_3$ (B). The ITC data of the interaction between MMP 2 and the PPEKEKPLGVRCCC (C). CD spectra of PPEKEKPLGVRCCC (red curve) and a mixture of MMP 2 and PPEKEKPLGVRCCC (green curve) (D).

various electrode interfaces was evaluated using lysozyme (Lyz), myoglobin (Mb), and BSA proteins with distinct charges. After incubation in protein solutions, the polypeptide-modified electrode demonstrated a significantly smaller change in current signal compared with the bare electrode (Figure 6C). This result demonstrated that the polypeptide had effective antifouling properties. Water contact angle analysis demonstrated a reduction from 53.3° to 17.9° for the

https://doi.org/10.1021/acs.analchem.5c02007
Anal. Chem. 2025, 97, 14574−14583

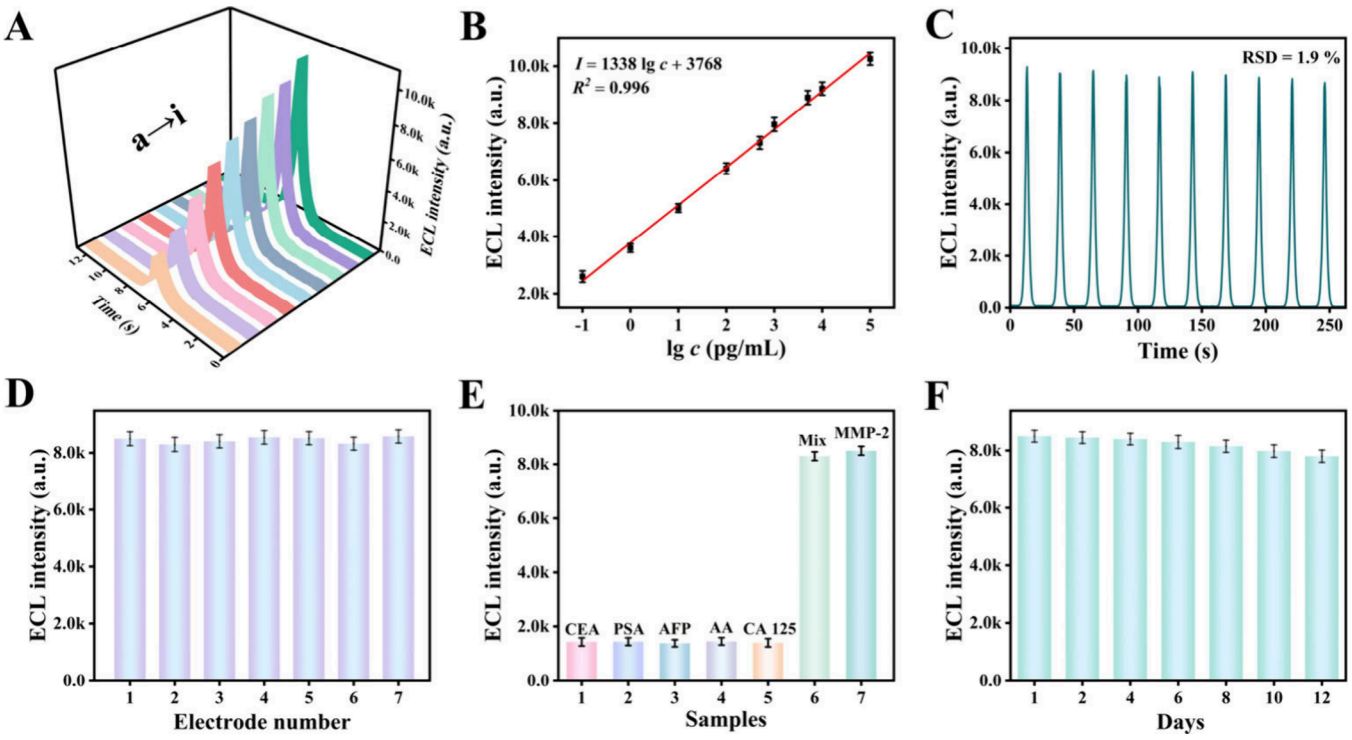

Figure 8. ECL signals for the various concentrations of MMP 2 (a−i: 0.1, 1, 10, 100, and 500 pg/mL, 1, 5, 10, and 100 ng/mL) (A). Standard curves for different concentrations of MMP 2 (B). Operational stability (C), reproducibility (D), selectivity (E), and storage stability (F) of the constructed sensor. Error bars: ± standard deviation (SD), n = 3.

polypeptide-modified electrode relative to the bare electrode (Figure 6D and Table S1). These results indicated that the polypeptide exhibited an excellent hydrophilicity.

Feasibility of Constructing MMP 2 Sensor. The zeta potentials of $Au_3Ag_5(MSA)_3$, Biotin−PPEKEKPLGVRCCC and Biotin−PPEKEKPLGVRCCC-$Au_3Ag_5(MSA)_3$ were tested, respectively. As shown in Figure 7B, $Au_3Ag_5(MSA)_3$ was negatively charged and had a potential of about −14 mV. The polypeptide chain was negatively charged and had a potential of around −19 mV. When $Au_3Ag_5(MSA)_3$ was mixed with Biotin−PPEKEKPLGVRCCC, the zeta potential value of the mixture showed a more negative potential of −28 mV. This showed that $Au_3Ag_5(MSA)_3$ was successfully connected to polypeptide.

Isothermal Titration Calorimetry (ITC) is a commonly used biophysical experimental technique that studies the interactions between biomolecules by measuring the process of heat exchange between them.[38] MMP 2 specifically cut fragments in Biotin−PPEKEKPLGVRCCC-$Au_3Ag_5(MSA)_3$, causing the segment of VRCCC-$Au_3Ag_5(MSA)_3$ to fall off (Figure 7A). The interaction between MMP 2 and polypeptide was detected by ITC. As shown in Figure 7C, the interaction between them was accompanied by changes in heat energy and was an endothermic reaction. The reaction was driven by entropy, which proved that MMP 2 effectively cleaved the polypeptide. Circular dichroism (CD) of polypeptide and the mixture of polypeptide and MMP 2 were measured simultaneously (Figure 7D). The intensity of the random crimp peak at 198 nm was increased for the CD of polypeptide−MMP 2 compared with that of the polypeptide. This observation indicated an increase in structural disorder within the polypeptide, suggesting that it is effectively cleaved by MMP 2.[39] At the same time, ECL was used to characterize the feasibility of the sensor. According to Figure S7, when MMP 2 was replaced by 50 μL of PBS, the ECL signal did not significantly change in the operating steps of the sensor platform. However, upon the addition of 1 ng/mL of MMP 2, an increase in the ECL signal was observed. This suggested that the polypeptide underwent cleavage, leading to the subsequent release of the VRCCC-$Au_3Ag_5(MSA)_3$ fragment. This finding served as evidence of the successful construction of the sensor.

Performance Testing of the ECL Sensor. ECL signals at different concentrations of MMP 2 were measured (Figure 8A). With the increase of MMP 2 concentration, ECL signal intensity also increased. The ECL signal and the logarithm of MMP 2 concentration present a good linear relationship over a range from 0.1 pg/mL to 100 ng/mL (Figure 8B), whose equation is I = 1338 lg$c$ + 3768, and the correlation coefficient (R^2) was 0.996. The detection limit obtained was 0.06 pg/mL (S/N = 3), which was a low detection limit. The sensor had the highest sensitivity and detection limits compared with other detection methods (Table S2).

The specificity, stability, and reproducibility of the sensor are important indexes for evaluating immunosensors. The relative standard deviation (RSD) of the ECL intensity signal peak was as low as 1.9% after 10 cycles scanning of 10 ng/mL MMP 2 (Figure 8C). It indicated that it had excellent operational stability. As shown in Figure 8D, the RSD of the ECL signals across seven electrode batches was less than 5%, demonstrating good reproducibility of the sensor. Additionally, we evaluated the specificity using 10 ng/mL CEA (carcinoembryonic antigen), PSA (prostate specific antigen), AFP (alpha-fetoprotein), AA (ascorbic acid), and their mixtures. As can be seen from Figure 8E, when only MMP 2 and its mixtures with other substances were present, the ECL intensity of this

https://doi.org/10.1021/acs.analchem.5c02007
Anal. Chem. 2025, 97, 14574−14583

sensor exhibited a significant change. This observation indicated that the sensor demonstrated high specificity for MMP 2. In addition, the constructed sensor was stored for 12 days and its ECL signal was remeasured to observe the storage stability of the sensor (Figure 8F). After 1 week, the ECL signal changed to 91.8% of the original, indicating that the sensor had excellent storage stability. Furthermore, compared with conventional ECL immunosensors, this split-type sensor had higher sensitivity and better stability (Figure S8).

Analysis of Serum Samples. We evaluated the recovery rate of MMP 2 in human serum to assess the feasibility of this method for sample analysis. The processed human serum samples (see details in the Supporting Information) with MMP 2 at 1.50, 2.00, 2.50, and 3.00 ng/mL were analyzed using the method proposed in this work. After conducting five parallel experiments, the recoveries from standard additions ranged from 98.6% to 101.6%. The RSD values were observed to range from 1.2% to 2.1% (Table S3). To assess the assay's accuracy, the ECL sensor was evaluated against the conventional ELISA. With a 95% confidence interval, the measured *F*-values (ranging from 1.90 to 3.32) were consistently below the threshold of 6.39 ($F_{0.05,4,4}$ = 6.39), demonstrating comparable precision between the two analytical approaches. Furthermore, *t* test analysis showed that the derived *t*-values (ranging from 0.71 to 0.95) were significantly lower than the reference value of 2.78 ($t_{0.05,4}$ = 2.78) (Table S4). The results indicated that the sensor was valuable for the analysis of MMP 2 in processed human serum samples.

CONCLUSION

In this study, we designed a split-type ECL sensing strategy for protease cutting polypeptide combined with bimetallic nanoclusters $Au_3Ag_5(MSA)_3$. Compared with traditional ECL immunosensors, this sensor was easier to operate and had better sensitivity and stability. Using $Au_3Ag_5(MSA)_3$ as the emitters of ECL sensors, the stability of the ECL signal and ECL efficiency were enhanced. The polypeptide can be specifically cut by MMP 2, thereby enhancing the sensor's specificity and facilitating productive detection of MMP 2. This provided a potential tool for clinical diagnosis and biological research.

ASSOCIATED CONTENT

Supporting Information

The Supporting Information is available free of charge at https://pubs.acs.org/doi/10.1021/acs.analchem.5c02007.

Reagents and materials, apparatus, preparation of MSA-Au NCs, ECL test parameters, construction of conventional ECL immunosensor, FL excitation spectra of $Au_3Ag_5(MSA)_3$, fluorescence lifetime of MSA-Au NCs, XPS spectra of the O 1s region and the C 1s region of $Au_3Ag_5(MSA)_3$, ECL−time curve of MSA-Au NCs, optimization of the incubation concentration and time of the peptides and nanoclusters, response changes of bare GCE and polypeptide with GCE, standard curves for different concentrations of MMP 2, performance testing of traditional ECL sensor, static water contact angles detection of MMP 2 in human serum samples, comparison with other analysis platforms for MMP 2 detection, pretreatments of serum sample, and comparison of the standard method (PDF)

AUTHOR INFORMATION

Corresponding Authors

Yu Du − *Collaborative Innovation Center for Green Chemical Manufacturing and Accurate Detection, Key Laboratory of Chemical Sensing & Analysis in Universities of Shandong, School of Chemistry and Chemical Engineering, University of Jinan, Jinan 250022, P. R. China;* orcid.org/0000-0002-9002-8845; Email: duyu_ujn@163.com

Xiaoyue Zhang − *Collaborative Innovation Center for Green Chemical Manufacturing and Accurate Detection, Key Laboratory of Chemical Sensing & Analysis in Universities of Shandong, School of Chemistry and Chemical Engineering, University of Jinan, Jinan 250022, P. R. China;* Email: ZXY881015@126.com

Qin Wei − *Collaborative Innovation Center for Green Chemical Manufacturing and Accurate Detection, Key Laboratory of Chemical Sensing & Analysis in Universities of Shandong, School of Chemistry and Chemical Engineering, University of Jinan, Jinan 250022, P. R. China; Department of Chemistry, Sungkyunkwan University, Suwon 16419, Republic of Korea;* orcid.org/0000-0002-3034-8046; Email: sdjndxwq@163.com

Authors

Qi Zhu − *Collaborative Innovation Center for Green Chemical Manufacturing and Accurate Detection, Key Laboratory of Chemical Sensing & Analysis in Universities of Shandong, School of Chemistry and Chemical Engineering, University of Jinan, Jinan 250022, P. R. China*

Xu Sun − *Collaborative Innovation Center for Green Chemical Manufacturing and Accurate Detection, Key Laboratory of Chemical Sensing & Analysis in Universities of Shandong, School of Chemistry and Chemical Engineering, University of Jinan, Jinan 250022, P. R. China;* orcid.org/0000-0001-8762-4243

Xiang Ren − *Collaborative Innovation Center for Green Chemical Manufacturing and Accurate Detection, Key Laboratory of Chemical Sensing & Analysis in Universities of Shandong, School of Chemistry and Chemical Engineering, University of Jinan, Jinan 250022, P. R. China;* orcid.org/0000-0002-4321-4282

Hongmin Ma − *Collaborative Innovation Center for Green Chemical Manufacturing and Accurate Detection, Key Laboratory of Chemical Sensing & Analysis in Universities of Shandong, School of Chemistry and Chemical Engineering, University of Jinan, Jinan 250022, P. R. China;* orcid.org/0000-0002-7061-8944

Dan Wu − *Collaborative Innovation Center for Green Chemical Manufacturing and Accurate Detection, Key Laboratory of Chemical Sensing & Analysis in Universities of Shandong, School of Chemistry and Chemical Engineering, University of Jinan, Jinan 250022, P. R. China;* orcid.org/0000-0002-8732-5988

Huangxian Ju − *Collaborative Innovation Center for Green Chemical Manufacturing and Accurate Detection, Key Laboratory of Chemical Sensing & Analysis in Universities of Shandong, School of Chemistry and Chemical Engineering, University of Jinan, Jinan 250022, P. R. China;* orcid.org/0000-0002-6741-5302

Complete contact information is available at: https://pubs.acs.org/10.1021/acs.analchem.5c02007

https://doi.org/10.1021/acs.analchem.5c02007
Anal. Chem. 2025, 97, 14574−14583

Notes

The authors declare no competing financial interest.

■ ACKNOWLEDGMENTS

This study was supported by the National Natural Science Foundation of China (Nos. 22274062, 22206056) and the Natural Science Foundation of Shandong Province (Nos. ZR2022QB117).

■ REFERENCES

(1) Fang, Y.; Li, Y.; Li, Y.; He, R.; Zhang, Y.; Zhang, X.; Liu, Y.; Ju, H. *Anal. Chem.* **2021**, *93* (19), 7258−7265.
(2) Hu, Q.; Su, L.; Mao, Y.; Gan, S.; Bao, Y.; Qin, D.; Wang, W.; Zhang, Y.; Niu, L. *Biosens. Bioelectron.* **2021**, *178*, No. 113010.
(3) Liu, F.; Chen, R.; Song, W.; Li, L.; Lei, C.; Nie, Z. *Anal. Chem.* **2021**, *93* (7), 3517−3525.
(4) Zhang, Q.; Chen, Z.; Shi, Z.; Li, Y.; An, Z.; Li, X.; Shan, J.; Lu, Y.; Liu, Q. *Biosens. Bioelectron.* **2021**, *193*, No. 113572.
(5) Duan, S.; Peng, J.; Cheng, H.; Li, W.; Jia, R.; Liu, J.; He, X.; Wang, K. *Talanta.* **2021**, *231*, No. 122418.
(6) Wu, F.; Huang, Y.; Yang, X.; Hu, J. J.; Lou, X.; Xia, F.; Song, Y.; Jiang, L. *Anal. Chem.* **2021**, *93* (48), 16257−16263.
(7) Li, T.; Cao, H.; Wu, S.; Zhong, P.; Ding, J.; Wang, J.; Wang, F.; He, Z.; Huang, G.-L. *J. Transl. Med.* **2022**, *20* (169), 169.
(8) Kacar, S.; Hacioglu, C.; Kar, F. *J. Cell. Mol. Med.* **2024**, *28* (8), e18288.
(9) Schreckenberg, R.; Schulz, R.; Itani, N.; Ferdinandy, P.; Bencsik, P.; Szabados, T.; Rohrbach, S.; Niemann, B.; Schlüter, K.-D. *Redox. Biol.* **2024**, *76*, No. 103308.
(10) Guo, Y. Z.; Yang, Y. T.; Chen, Y. F.; Liu, J. L.; Chai, Y. Q.; Yuan, R. *Anal. Chem.* **2023**, *95* (17), 7021−7029.
(11) Li, J.; Li, Y.; Xu, L.; Fang, X.; Yin, H.; Xu, Q.; Fang, H.; Li, H.; Wang, W. *Sensor. Actuat. B-Chem.* **2020**, *320*, 128597.
(12) Xie, X.; Sun, Y.; Peng, J.; Zhang, Z.; Wang, M.; Wang, Z.; Lei, C.; Huang, Y.; Nie, Z. *Anal. Chem.* **2023**, *95* (50), 18487−18496.
(13) Liu, L.; Chu, H.; Yang, J.; Sun, Y.; Ma, P.; Song, D. *Biosens. Bioelectron.* **2022**, *212*, No. 114389.
(14) Nie, Y.; Zhang, P.; Wang, H.; Zhuo, Y.; Chai, Y.; Yuan, R. *Anal. Chem.* **2017**, *89* (23), 12821−12827.
(15) Ma, X.; Kang, Q.; Li, M.; Fu, L.; Zou, G.; Shen, D. *Anal. Chem.* **2022**, *94* (8), 3637−3644.
(16) Zhang, H.; Wu, M.; Ta, H. T.; Xu, Z. P.; Zhang, R. *Adv. Mater. Technol.* **2023**, *8* (9), No. 2201786.
(17) Mei, X.; Wang, W.; Bu, L.; Li, Q.; Jiang, D.; Wu, M.; Chen, Z. *Microchem. J.* **2023**, *195*, No. 109451.
(18) Wang, X.-Y.; Che, Z.-Y.; Bao, N.; Qing, Z.; Ding, S.-N. *Talanta Open.* **2022**, *5*, No. 100088.
(19) Lin, S.; Zheng, S.; Wu, H.; Zhang, Z.; Xie, X.; Yang, P.; Huang, Y.; Li, F. *Anal. Chem.* **2023**, *95* (23), 9116−9122.
(20) Li, J.; Xi, M.; Hu, L.; Sun, H.; Zhu, C.; Gu, W. *Anal. Chem.* **2024**, *96* (5), 2100−2106.
(21) Ru, Z.; Jia, Y.; Du, Y.; Han, Y.; Zhang, N.; Ren, X.; Wei, Q. *Anal. Chem.* **2023**, *95* (27), 10178−10185.
(22) Song, X.; Wu, T.; Luo, C.; Zhao, L.; Ren, X.; Zhang, Y.; Wei, Q. *Anal. Chem.* **2021**, *93* (38), 13045−13053.
(23) Han, S.; Zhang, Z.; Li, S.; Qi, L.; Xu, G. *Sci. China Chem.* **2016**, *59* (7), 794−801.
(24) Liu, Q.; Yan, X.; Lai, Q.; Su, X. *Sensor. Actuat. B-Chem.* **2019**, *282*, 45−51.
(25) Fu, L.; Gao, X.; Dong, S.; Hsu, H.-Y.; Zou, G. *Anal. Chem.* **2021**, *93* (11), 4909−4915.
(26) Liu, X.; Zhang, X.; Feng, R.; Ren, X.; Wu, D.; Liu, X.; Liu, L.; Wei, Q. *Anal. Chem.* **2024**, *96* (21), 8390−8398.
(27) Chen, S.; Ma, H.; Padelford, J. W.; Qinchen, W.; Yu, W.; Wang, S.; Zhu, M.; Wang, G. *J. Am. Chem. Soc.* **2019**, *141* (24), 9603−9609.
(28) Ge, X.; Zhang, M.; Yin, F.; Sun, Q.; Mo, F.; Huang, X.; Zheng, Y.; Wu, G.; Zhang, Y.; Shen, Y. *J. Mater. Chem. B* **2024**, *12* (5), 1355−1360.
(29) Liu, J.; Zhao, R.; Wang, X.; Gao, X.; Zou, G. *Chem. Commun.* **2020**, *56* (42), 5665−5668.
(30) Khan, I. M.; Niazi, S.; Yu, Y.; Mohsin, A.; Mushtaq, B. S.; Iqbal, M. W.; Rehman, A.; Akhtar, W.; Wang, Z. *Anal. Chem.* **2019**, *91* (21), 14085−14092.
(31) Jia, H.; Yang, L.; Fan, D.; Kuang, X.; Sun, X.; Wei, Q.; Ju, H. *Sensor. Actuat. B-Chem.* **2022**, *367*, No. 132034.
(32) Liu, N.; Song, J.; Lu, Y.; Davis, J. J.; Gao, F.; Luo, X. *Anal. Chem.* **2019**, *91* (13), 8334−8340.
(33) Chen, L.; Du, Y.; Lv, Y.; Fan, D.; Wu, J.; Wu, L.; Cui, M.; Yu, H.; Zhu, M. *Nano Res.* **2023**, *16* (5), 7770−7776.
(34) Tan, Y.; Huang, D.; Luo, C.; Tang, J.; Kwok, R. T. K.; Lam, J. W. Y.; Sun, J.; Liu, J.; Tang, B. Z. *Nano Lett.* **2023**, *23* (16), 7683−7690.
(35) Jia, H.; Yang, L.; Dong, X.; Zhou, L.; Wei, Q.; Ju, H. *Anal. Chem.* **2022**, *94* (4), 2313−2320.
(36) Zhang, D.; Cao, C.; Chen, Q.; Liu, J.; Liu, H.; Liu, Y.; Yuan, Y.; Liu, H.; Lin, H.; Liu, R. *Appl. Mater. Today.* **2022**, *27*, No. 101511.
(37) Li, Y.; Chen, Z.; Li, W.; Zhang, F.; Yang, X.; Ding, C. *Talanta.* **2024**, *267*, No. 125229.
(38) Manka, S. W.; Brew, K. *J. Mol. Biol.* **2020**, *432* (22), 5985−5993.
(39) Patkar, S. S.; Tang, Y.; Zhang, T.; Bisram, A. M.; Saven, J. G.; Pochan, D. J.; Kiick, K. L. *Biomacromolecules.* **2024**, *25* (4), 2449−2461.

https://doi.org/10.1021/acs.analchem.5c02007
Anal. Chem. 2025, 97, 14574−14583